0.04; mean age 42±11 years, n=169) reported by Yaldizli et al. (19). Therefore, we think that CCA should be monitored more carefully in HDLS patients.

The LADIS study indicated that CCA is associated with cognitive decline that coexists independently with white matter hyperintensity and stroke (23, 24). In particular, overall CCA is correlated with the slowing of processing or mental speed (23, 24). In patients with HDLS, frontal lobe signs and symptoms are frequently observed in the early stage of the disease. This is consistent with the observation of Sundal et al. that WMLs are predominantly frontal (3), as supported by the findings of this study. Additionally, it is possible that the early involvement of the CC contributes to the psychomotor dysfunction observed in HDLS patients.

CCA is observed in elderly persons, as well as in patients with cerebrovascular and neurodegenerative diseases (25-31). Several underlying mechanisms for CCA have been postulated (25-30). In Alzheimer's disease patients, CCA primarily reflects the loss of the corresponding cortical neurons (Wallerian degeneration hypothesis) (26, 28, 29) and/or age-related myelin breakdown (retrogenesis hypothesis) (28, 29, 32). Conversely, in patients with cerebrovascular diseases, CCA is closely related to cerebral WMLs (26, 27, 31), assuming that ischemic damage causes focal edema and inflammation with subsequent axonal disruption (26). The mechanism underlying the development of CCA in patients with HDLS is likely to be different from that observed in those with Alzheimer's disease or cerebrovascular disease because CCA develops in the earlier stage of the disease and progresses more rapidly in HDLS.

HDLS is neuropathologically characterized by the extensive loss of myelin sheaths, axonal destruction and the presence of numerous axonal spheroids, pigmented macrophages and astrogliosis (2, 9-14). These changes were clearly observed in the centrum semiovale of the cerebral white matter in one of our patients (patient 2) (8). That patient died of sepsis caused by severe intestinal infection at age 41 in the early stage of the disease (mRS3). Macroscopically, the CC was diffusely thin (data not shown). Histologically, the localized portion of the splenium of the CC that exhibited T2 and FLAIR high signals on MRI demonstrated a severe loss of myelin and axons with axonal spheroids, as seen in the centrum semiovale. This is a primary pathological process of axonal disruption in HDLS. On the other hand, the basic structure was relatively preserved in the other parts of the CC, where the number of axons was decreased; however, the findings of tissue destruction, including localized myelin loss, disarrangement of axons and the presence of spheroids and activated macrophages, were quite mild. This likely reflects a secondary change due to axonal damage in the proximal parts of the commissural fibers. CC involvement in HDLS patients is therefore considered to be caused by these combined pathological processes. Additionally, ischemic changes, including small infarcts and microvascular fibrohyalinosis, were almost absent in the entire CC; therefore, the pathologic mechanism appears to be basically different between HDLS and cerebrovascular disease.

The present study is associated with several limitations. First, the number of HDLS patients was very small. The incidence of HDLS in the Japanese population remains unknown because genetic testing for *CSF1R* has only recently been introduced into clinical practice, and genetically-proven cases are very small in number at present. Second, the patients in the VaD group in this study were rather heterogeneous because this was a retrospective study. The mRS of the VaD group (2.75±0.89) was not significantly different from that of the HDLS group (3.30±1.10); however, the cognitive function levels varied from subnormal to severe dementia in the VaD group. As judged according to the mRS, cognitive, mental and motor dysfunction was variable in both the HDLS and VaD groups; therefore, it was not possible to make MRI comparisons between these two groups after adjusting for the clinical status. Third, there was overlap in the values of the CCI between the HDLS and VaD patients; therefore, we were unable to present any diagnostic cutoff values for distinguishing HDLS from VaD.

In conclusion, despite the several limitations described above, our quantitative neuroimaging study clearly showed the presence of CCA on the initial MRI scans (6-36 months after disease onset) in HDLS patients. Our findings suggest that the presence of CCA on MRI frequently accompanied by high intensity in the genu and/or splenium on T2 and FLAIR images is a useful finding indicative of HDLS.

The authors state that they have no Conflict of Interest (COI).

Acknowledgement

We thank the two examiners (Mr. Yusuke Takahashi and Mr. Kazuhito Takahashi) for their assistance in measuring the MR images. This work was supported by Grants-in-Aid from the Research Committee for hereditary cerebral small vessel disease and associated disorders of the Ministry of Health, Labour and Welfare of Japan (Dr. Kunihiro Yoshida).

References

1. Rademakers R, Baker M, Nicholson AM, et al. Mutations in the colony stimulating factor 1 receptor (*CSF1R*) gene cause hereditary diffuse leukoencephalopathy with spheroids. Nat Genet **44**: 200-205, 2012.
2. Wider C, Van Gerpen JA, DeArmond S, Shuster EA, Dickson DW, Wszolek ZK. Leukoencephalopathy with spheroids (HDLS) and pigmentary leukodystrophy (POLD). A single entity? Neurology **72**: 1953-1959, 2009.
3. Sundal C, Van Gerpen JA, Nicholson AM, et al. MRI characteristics and scoring in HDLS due to *CSF1R* gene mutations. Neurology **79**: 566-574, 2012.
4. Moro-de-Casillas ML, Cohen ML, Riley DE. Leucoencephalopathy with neuroaxonal spheroids (LENAS) presenting as the cerebellar subtype of multiple system atrophy. J Neurol Neurosurg Psychiatry **75**: 1070-1072, 2004.
5. Keegan BM, Giannini C, Parisi JE, Lucchinetti CF, Boeve BF, Josephs KA. Sporadic adult-onset leukoencephalopathy with neuroaxonal spheroids mimicking cerebral MS. Neurology **70**: 1128-1133, 2008.
6. Wong JC, Chow TW, Hazrati L-N. Adult-onset leukoencephalopa-

thy with axonal spheroids and pigmented glia can present as frontotemporal dementia syndrome. Dement Geriatr Cogn Disord **32**: 150-158, 2011.

7. Sundal C, Lash J, Aasly J, et al. Hereditary diffuse leukoencephalopathy with axonal spheroids (HDLS): A misdiagnosed disease entity. J Neurol Sci **314**: 130-137, 2012.
8. Kondo Y, Kinoshita M, Fukushima K, Yoshida K, Ikeda S. Early involvement of the corpus callosum in a patient with hereditary diffuse leukoencephalopathy with spheroids carrying the *de novo* K793T mutation of *CSF1R*. Intern Med **52**: 503-506, 2013.
9. van der Knaap MS, Naidu S, Kleinschmidt-Demasters BK, Kamphorst W, Weinstein HC. Autosomal dominant diffuse leukoencephalopathy with neuroaxonal spheroids. Neurology **54**: 463-468, 2000.
10. Terada H, Ishizu H, Yokota O, et al. An autopsy case of hereditary diffuse leukoencephalopathy with spheroids, clinically suspected of Alzheimer's disease. Acta Neuropathol **108**: 538-545, 2004.
11. Marotti JD, Tobias S, Fratkin JD, Powers JM, Rohdes CH. Adult onset leukodystrophy with neuroaxonal spheroids and pigmented glia: report of a family, historical perspective, and review of the literature. Acta Neuropathol **107**: 481-488, 2004.
12. Itoh K, Shiga K, Shimizu K, Muranishi M, Nakagawa M, Fushiki S. Autosomal dominant leukodystrophy with axonal spheroids and pigmented glia: clinical and neuropathological characteristics. Acta Neuropathol **111**: 39-45, 2006.
13. Baba Y, Ghetti B, Baker MC, et al. Hereditary diffuse leukoencephalopathy with spheroids: clinical, pathologic and genetic studies of a new kindred. Acta Neuropathol **111**: 300-311, 2006.
14. Freeman SH, Hyman BT, Sims KB, Hedley-Whyte ET, Vossough A, Frosch MP. Adult onset leukodystrophy with neuroaxonal spheroids: clinical, neuroimaging and neuropathologic observations. Brain Pathol **19**: 39-47, 2009.
15. Kinoshita M, Yoshida K, Oyanagi K, Hashimoto T, Ikeda S. Hereditary diffuse leukoencephalopathy with axonal spheroids caused by R782H mutation in *CSF1R*: case report. J Neurol Sci **318**: 115-118, 2012.
16. Román GC, Tatemichi TK, Erkinjuntti T, et al. Vascular dementia: diagnostic criteria for research studies. Report of the NINDS-AIREN International Workshop. Neurology **43**: 250-260, 1993.
17. Sulter G, Steen C, De Keyser J. Use of the Barthel index and modified Rankin scale in acute stroke trial. Stroke **30**: 1538-1541, 1999.
18. Figueira FFA, dos Santos VS, Figueira GMA, da Silva ÂCM. Corpus callosum index: a practical method for lomg-term follow-up in multiple sclerosis. Arq Neuropsiquiatr **65**: 931-935, 2007.
19. Yaldizli O, Atefy R, Gass A, et al. Corpus callousm index and long-term disability in multiple sclerosis patients. J Neurol **257**: 1256-1264, 2010.
20. Takeda S, Hirashima Y, Ikeda H, Yamamoto H, Sugino M, Endo S. Determination of indices of the corpus callosum associated with normal aging in Japanese individuals. Neuroradiol **45**: 513-518, 2003.
21. Yamashita M, Yamamoto T. Neuroaxonal leukoencephalopathy with axonal spheroids. Eur Neurol **48**: 20-25, 2002.
22. Oishi M, Mochizuki Y, Shikata E. Corpus callosum atrophy and cerebral blood flow in chronic alcoholics. J Neurol Sci **162**: 51-55, 1999.
23. Jokinen H, Ryberg C, Kalska H, et al; LADIS group. Corpus callosum atrophy is associated with mental slowing and executive deficits in subjects with age-related white matter hyperintensities: the LADIS study. J Neurol Neurosurg Psychiatr **78**: 491-496, 2007.
24. Jokinen H, Frederiksen KS, Garde E, et al. Callosal tissue loss parallels subtle decline in psychomotor speed. a longitudinal quantitative MRI study. The LADIS Study. Neuropsychologia **50**: 1650-1655, 2012.
25. Meguro K, Constans JM, Courtheoux P, Theron J, Viader F, Yamadori A. Atrophy of the corpus callosum correlates with white matter lesions in patients with cerebral ischaemia. Neuroradiology **42**: 413-419, 2000.
26. Tomimoto H, Lin JX, Matsuo A, et al. Different mechanisms of corpus callosum atrophy in Alzheimer's disease and vascular dementia. J Neurol **251**: 398-406, 2004.
27. Ryberg C, Rostrup E, Sjöstrand K, et al; LADIS study group. White matter changes contribute to corpus callosum atrophy in the elderly: the LADIS study. AJNR Am J Neuroradiol **29**: 1498-1504, 2008.
28. Di Paola M, Di Iulio F, Cherubini A, et al. When, where, and how the corpus callosum changes in MCI and AD: a multimodel MRI study. Neurology **74**: 1136-1142, 2010.
29. Di Paola M, Luders E, Di Iulio F, et al. Callosal atrophy in mild cognitive impairment and Alzheimer's disease: different effects in different stages. Neuroimage **49**: 141-149, 2010.
30. Frederiksen KS, Garde E, Skimminge A, et al. Corpus callosum tissue loss and development of motor and global cognitive impairment: the LADIS study. Dement Geriatr Cogn Disord **32**: 279-286, 2011.
31. Lee DY, Fletcher E, Martinez O, et al. Vascular and degenerative processes differentially affect regional interhemispheric connections in normal aging, mild cognitive impairment, and Alzheimer disease. Stroke **41**: 1791-1797, 2010.
32. Bartzokis G. Age-related myelin breakdown: a development model of cognitive decline and Alzheimer's disease. Neurobiol Aging **25**: 5-18, 2004.

© 2014 The Japanese Society of Internal Medicine
http://www.naika.or.jp/imonline/index.html

Neuroradiology (2013) 55:283–290
DOI 10.1007/s00234-012-1105-x

DIAGNOSTIC NEURORADIOLOGY

Detection of early neuronal damage in CADASIL patients by q-space MR imaging

Kei Yamada · Koji Sakai · Kentaro Akazawa · Naozo Sugimoto · Masanori Nakagawa · Toshiki Mizuno

Received: 25 July 2012 / Accepted: 5 October 2012 / Published online: 25 October 2012
© Springer-Verlag Berlin Heidelberg 2012

Abstract
Introduction q-Space imaging is a novel magnetic resonance (MR) technique that enables the assessment of ultrastructural changes of white matter. We hypothesized that this technique would facilitate the assessment of the progressive nature of neuronal damage seen in cerebral autosomal dominant arteriopathy with subcortical infarcts and leukoencephalopathy (CADASIL).
Methods This study was approved by the institutional review board. Seven consecutive adult patients (five men and two women) with the CADASIL gene mutation were studied. Two patients were preclinical cases without overt episodes of stroke. The control group consisted of five normal volunteers. All MR examinations were performed using a 1.5-T whole-body imager. q-Space imaging was performed using a single-shot, echo-planar imaging technique and Δ/δ=142/17 ms. Gradient magnitudes were increased in nine steps to reach a maximal b value of 10,000 s/mm^2. Total acquisition time of q-space imaging was 25 min. The ADC maps calculated from the b=1,000 images were used for comparisons.
Results Both q-space imaging and ADC maps depicted progressive neuronal damage. Early neuronal damage was especially well depicted using q-space imaging, with preferential involvement of the frontal lobes and central gray matters. Later progression was better depicted by b=1,000 ADC maps at the temporal lobes. Visual assessment of images revealed a trend for occipital lobe sparing, especially on q-space imaging.
Conclusion q-Space imaging demonstrated early neuronal damage in a characteristic distribution. Since this method appears to be sensitive to early neuronal damage, it could conceivably aid in monitoring patients in the preclinical stage and may help in assessing the effects of future medical interventions.

Keywords CADASIL · White matter · Diffusion-weighted imaging · q-Space imaging · Mean displacement (MD)

Abbreviations

CC	Corpus callosum
CGM	Central gray matters
MD	Mean displacement
SPG	Short pulse gradient

Introduction

Cerebral autosomal dominant arteriopathy with subcortical infarcts and leukoencephalopathy (CADASIL) is a hereditary condition causing recurrent subcortical strokes. It is caused by mutations in the notch3 gene. Recurrent vascular events, headache, mood disorders, and progressive cognitive decline are the main clinical manifestations. Histopathological studies have indicated that the characteristic features are arteriopathy of small- and middle-sized arteries without atherosclerosis or amyloid deposition. This arteriopathy results in an "earthen pipe state," by which cerebral autoregulation is lost [1]. This

K. Yamada (✉) · K. Akazawa
Department of Radiology, Graduate School of Medical Science,
Kyoto Prefectural University of Medicine,
Kajii-cho, Kawaramachi Hirokoji Sagaru, Kamigyo-ku,
Kyoto City, Kyoto 602-8566, Japan
e-mail: kyamada@koto.kpu-m.ac.jp

M. Nakagawa · T. Mizuno
Department of Neurology, Graduate School of Medical Science,
Kyoto Prefectural University of Medicine,
Kajii-cho, Kawaramachi Hirokoji Sagaru, Kamigyo-ku,
Kyoto City, Kyoto 602-8566, Japan

K. Sakai · N. Sugimoto
Department of Human Health Science,
Graduate School of Medicine, Kyoto University,
53 Shogoin Kawara-cho, Sakyo-ku,
Kyoto City, Kyoto 606-8507, Japan

leads to ischemia, demyelination, and reactive gliosis, with relative sparing of the subcortical U-fibers [1].

Neuroimaging shows both focal lacunar infarcts and diffuse white matter ischemic changes. Magnetic resonance (MR) imaging is especially useful and plays an important initial role in the diagnosis, since studies have demonstrated characteristic features, such as involvement of the anterior temporal pole and external capsule [2].

Another potential role of imaging is to monitor disease progression. However, the progression of white matter damage on fluid attenuated inversion recovery (FLAIR) images typically levels off at the fifth decade, when hyperintense lesions become widespread throughout the cerebral white matter [3]. Furthermore, there is no established neuroimaging technique that enables monitoring of patients in the preclinical stage. Thus, an imaging method that would enable better characterization of the brain at the earliest stage would be of clinical benefit.

Assessment of the disease status of CADASIL patients has been attempted by the use of diffusion-weighted imaging (DWI) and diffusion tensor imaging (DTI) techniques [4]. These depict tissue damage through ADC measurements even in areas that appear normal on conventional MR [5]. Furthermore, the DTI histogram metrics have been shown to be more sensitive than conventional imaging studies in predicting disease progression [4].

Recent studies have further extended the conventional DTI technique to use much higher b values (e.g., 10,000 s/mm^2) [6–9]. The method is known as q-space imaging; it was originally designed to measure the compartment size of porous material filled with water [6]. Owing to various technical challenges, it was initially limited to study animals [10–13], but was later extended to clinical imaging [14–17]. This technique with high b values enables measurement of the mean displacement (MD) of the most slowly diffusing water molecules. By applying this technique to the central nervous system, one can now perform ultrastructural assessment of the compartment size of white matter [10, 11, 14, 18]. For instance, excellent agreements have been found between axonal size as obtained on q-space imaging and histology of optic nerves and the spinal cord [19, 20].

The aim of this study was to test the feasibility of this novel technique to assess the neuronal damage in CADASIL patients. More specifically, whether one could better observe the progressive nature of neuronal damage in CADASIL patients was examined.

Methods

Patient population

This study was approved by the institutional review board. Seven consecutive adult patients (five men and two women) ranging in age from 44 to 76 (mean, 55) years were studied. All of these patients were genetically proven to have CADASIL through direct sequencing (i.e., NOTCH3 mutations including C106R, R141C, or R332C). All of them had cerebral white matter lesions on FLAIR to various extents. The study period was from August 2010 to April 2011. The control group consisted of five subjects (mean age, 41 years; four men and one woman) who volunteered. None of them had a history of neurological disease or head trauma. All were in excellent health, and they did not exhibit any white matter lesions on MR.

Data acquisition

All MR examinations were performed using a 1.5-T whole-body imager (Philips Medical Systems, Best, the Netherlands). In all MRI scans, the field of view was 23 cm. DWI for q-space imaging was acquired using a single-shot, echo-planar imaging technique [repetition time (TR)/echo time

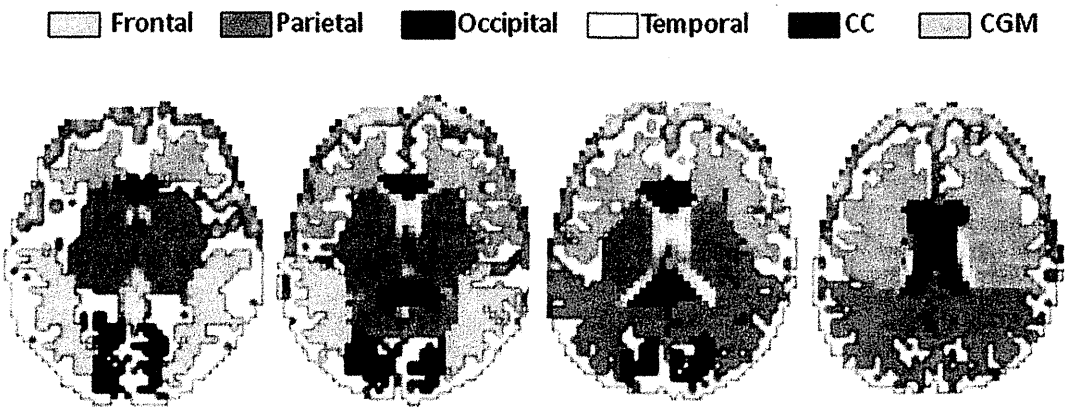

Fig. 1 Template for ROI analysis. Manual segmentation of the white matter of four lobes, corpus callosum, and CGM was performed as indicated in this figure

(TE)=6,000/173 ms], Δ/δ=142/17 ms (effective diffusion time (T_{diff})=136 ms) and a matrix of 128×128, without cardiac gating. Gradient magnitudes were increased in nine steps to reach a maximal b value of 10,000 s/mm^2 and a maximal q value of 855 cm^{-1}. The b values used were 0, 10, 60, 100, 300, 600, 1,000, 3,000, 6,000, and 10,000 s/mm^2. Motion-sensitizing gradients were applied in 15 directions. A total of twelve 3-mm-thick sections were obtained without intersection gaps to cover the central parts of the brain, including the basal ganglia and the upper limit of the corpus callosum. These diffusion-weighted images were motion/distortion corrected to match the b=0 images on the console of the MR unit. The q-space data set included 136 images per slice (nine diffusion images in 15 diffusion gradient directions) with total acquisition time of 25 min.

Data postprocessing

Data were sent to an offline computer for further analysis on a homemade software. The q-space analysis was performed on a pixel-by-pixel basis, as previously described [14]. High b value components above 10,000 s/mm^2 were zero-filled upon the analysis. First, the mean displacement distribution profile was calculated for each gradient direction by Fourier transformation of the signal decay. The full width at half maximum of the displacement distribution profile was then

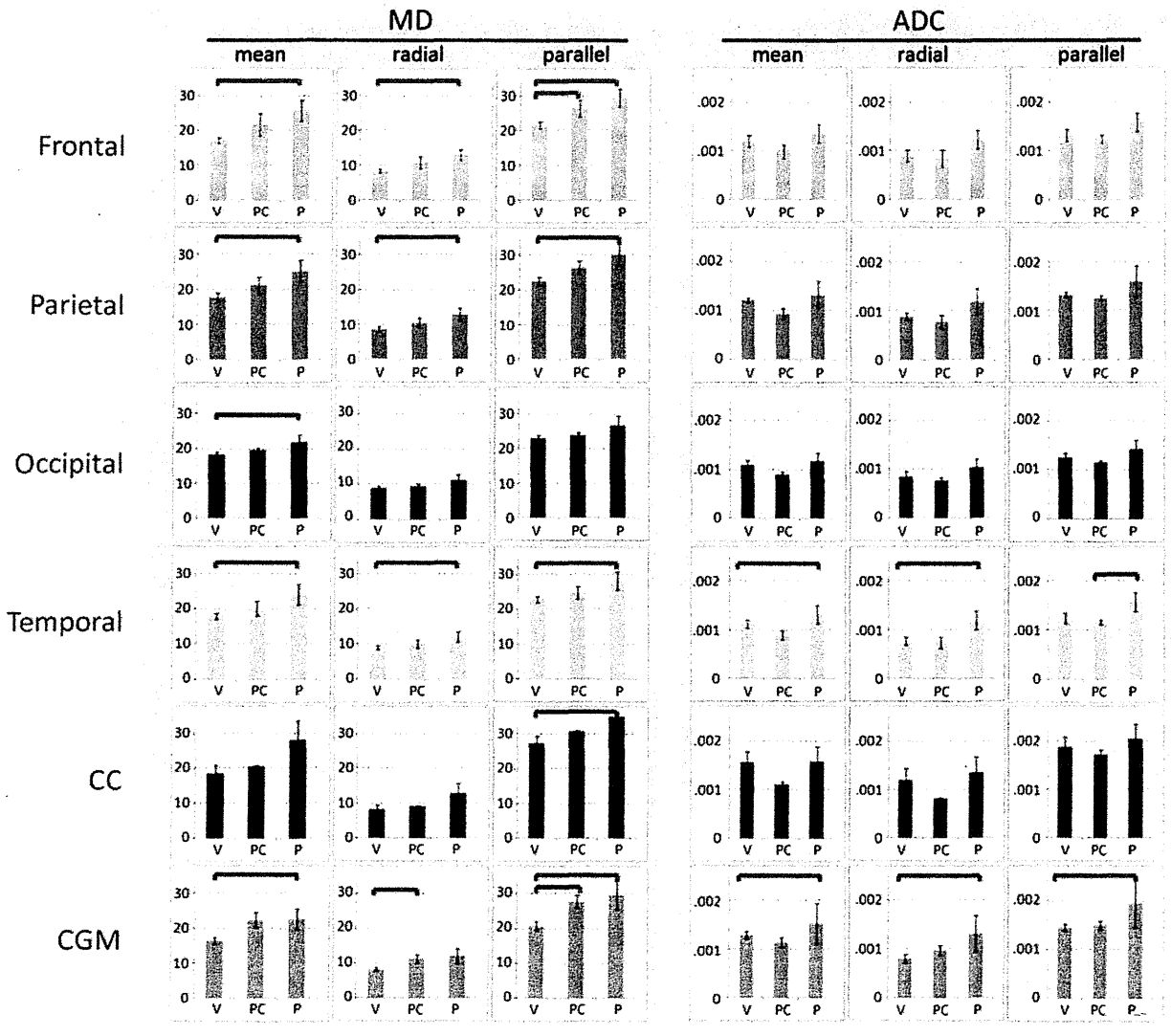

Fig. 2 Comparisons of normal volunteers (*V*), preclinical CADASIL patients (*PC*), and CADASIL patients (*P*). Substantial differences are noted in various locations, and the differences between normal and preclinical patients are most apparent using minimum mean displacement (*MD*) maps. *Frontal* frontal lobe, *Parietal* parietal lobe, *Occipital* occipital lobe, *Temporal* temporal lobe; *CC* corpus callosum; *CGM* central gray matter

calculated, and these values were used to represent the MD [14]. After this calculation, a tensor analysis was performed on MD for each voxel. The radial and parallel components of this tensor (MD_{radial} and $MD_{parallel}$) were also calculated. The ADC and the radial/parallel components of ADC (ADC_{radial} and $ADC_{parallel}$) were calculated from b=0 and b=1,000 s/mm^2.

ROI analysis

Region of interest (ROI) analysis was performed using manually segmented white matter of four lobes (e.g., frontal, parietal, occipital, and temporal lobes), corpus callosum, and central gray matter (Fig. 1). The ROI was defined on each subject by a single operator (KY) trained in neuroanatomy and neuroradiology. The patient's status was blinded when drawing these ROIs on the b=0 images. Signal-to-noise ratio was calculated by combining these ROIs with the denominator from the background ROI taken at the surrounding air of the head.

Statistics

Comparisons were performed using Student's t test (Matlab; The Mathworks, Natick, MA, USA) with Bonferroni corrections. The correlation was evaluated as significant for the P values of <0.005 for the comparison between the patients and healthy subjects and P values of <0.007 for the comparison between the preclinical (PC) subjects.

Visual assessment

Visual assessments of the images were carried out to further characterize the acquired maps of both normal volunteers and patients. This was done by the primary investigator (KY) of this study.

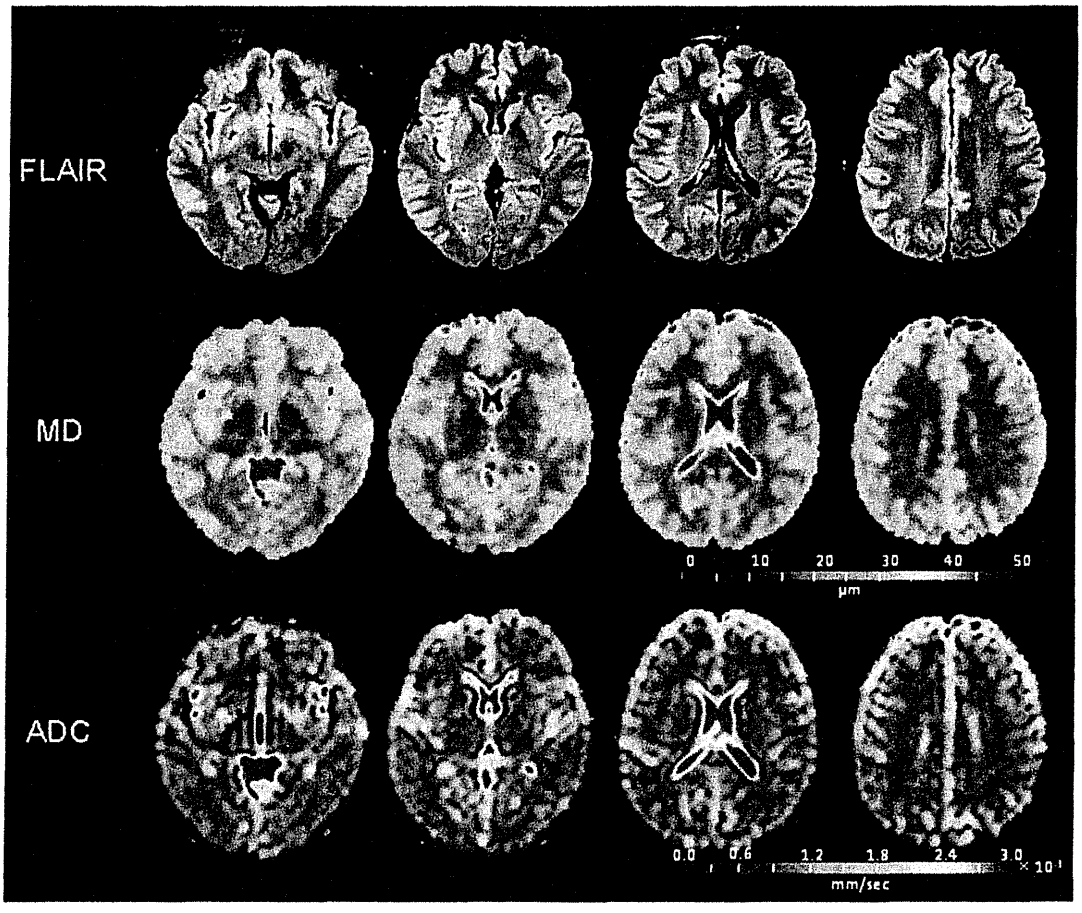

Fig. 3 Representative images from a normal volunteer. This is a 28-year-old man who volunteered to undergo the q-space imaging experiment. Note that, on the MD maps, there is clear definition between the cerebral cortex and underlying white matter. This is in contrast with the ADC maps that do not show a clear difference between the two structures

Results

ROI analysis

q-Space imaging was successfully carried out in all patients and volunteers, and the MD and ADC maps were generated from these data sets. The average signal-to-noise ratios (SNRs) for b=1,000 and b=10,000 were 16.3 and 9.1, respectively. The ROI analyses of these maps revealed substantial differences between the normal volunteers (V) and CADASIL patients (P) (Fig. 2). Statistically significant differences were noted at wider areas of the brain using q-space imaging than the ADC maps.

Some differences were also noted between the normal volunteers (V) and preclinical (PC) patients on MD_{radial} and $MD_{parallel}$. These differences were noted in the frontal white matter and central gray matters (CGM). Differences between the preclinical (PC) and symptomatic CADASIL patients (P) were noted in the temporal white matters on the ADC map (i.e., $ADC_{parallel}$) but not on MD maps.

Visual assessment

The MD maps of normal volunteers were characterized by white matter with uniformly low MD below 20 μm, represented by the blue color (Fig. 3). The cerebral cortex, on the other hand, had higher MD (shown by green color) with relatively well-defined contrast between the cortex and underlying white matter. This gray/white contrast was not clear on the ADC maps. The mean diffusivity of CGM was similar to the surrounding white matter.

Visual assessment of the MD maps on preclinical CADASIL (Fig. 4) and CADASIL patients (Fig. 5) revealed that there was a substantial increase in MD of the white matter in widespread areas. The white matter damage was readily recognizable on MD maps even in the preclinical stage.

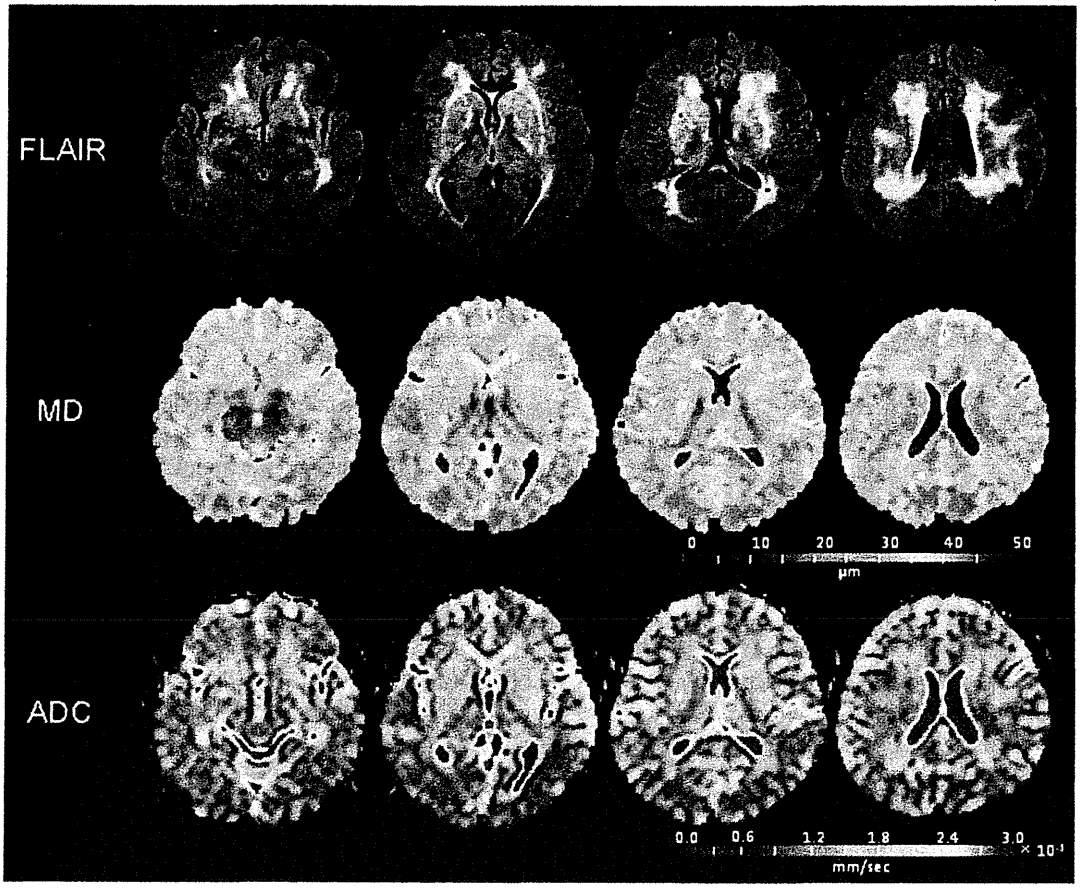

Fig. 4 Representative case of preclinical CADASIL. This is a 54-year-old man with CADASIL. The white matter damage is already apparent on the MD and ADC maps. Sparing of the U-fibers is also evident in some parts of the brain. Note that the posterior parts of the brain, including the occipital lobes, are relatively spared when compared with the other parts of brain. This trend of occipital lobe sparing is more clearly noted on the MD maps than the FLAIR

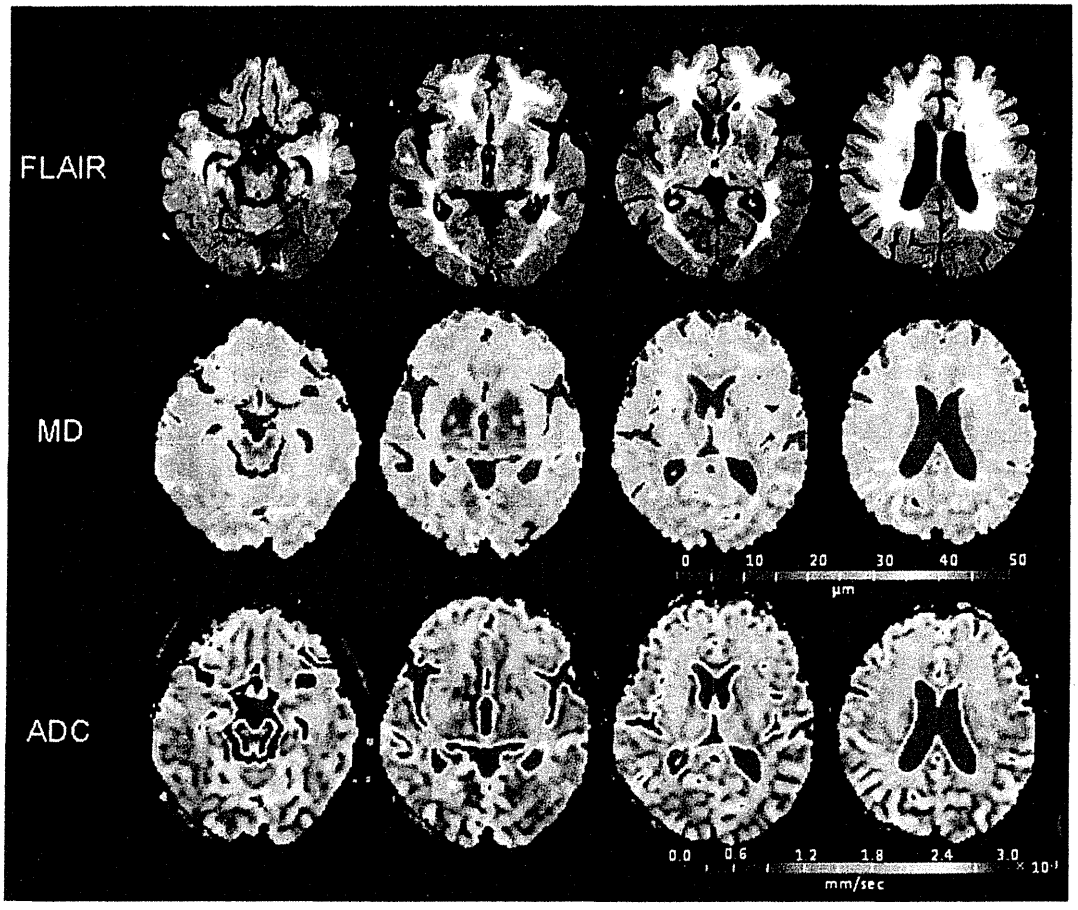

Fig. 5 Representative case of CADASIL. This is a 76-year-old man with full-blown CADASIL. The MD maps of q-space imaging reveal remarkable differences in the appearance of the white matter when compared with the normal volunteer and the preclinical case (Figs. 3 and 4). Sparing of the U-fibers is also evident in some parts of the brain, especially on ADC maps

There was also a trend for slight occipital lobe sparing, which was most apparent on MD maps even compared with the FLAIR.

Discussion

The results of the present study demonstrated that, using the q-space approach, the white matter damage in CADASIL patients could be readily visualized. Especially important could be the fact that it enables the observation of the earliest stage of neuronal damage. This implies the potential role of q-space imaging in assessing disease progression in preclinical patients. Preferential involvement of the fronto-parietal regions in the preclinical stage has been pointed out previously using MR imaging techniques, including MR spectroscopy and volumetric measurements [21]. This is in keeping with our ROI measurements.

In addition to these white matter regions, CGM was also severely affected already in the preclinical stage. It is well known from histological studies that the vessels most affected in CADASIL are the leptomeningeal and lenticulostriate arteries [22, 23]. Thus, the preferential involvement of the CGM in the present study was anticipated. It may be also noteworthy that despite such substantial changes at the CGM on q-space imaging, hyperintensity on FLAIR was not overt in some of the cases. For instance, as illustrated in Fig. 5, this particular CADASIL patient did not have significant hyperintensity at the thalami on FLAIR (Fig. 5). This superior sensitivity of q-space imaging to the CGM damages may be the potential advantage of this technique.

Since the q-space imaging technique appeared to be most sensitive to the early changes in the frontal lobes and CGM, these regions can be considered the potential target zones for monitoring the effect of future medical interventions. In order to test the potential role of q-space imaging as a monitoring tool, we are currently performing a longitudinal follow-up on our CADASIL population.

Degree of disease progression was examined by comparing the preclinical (PC) to symptomatic patients (P), as

shown in Fig. 2. Most characteristic was the progressive temporal lobe damage depicted by $ADC_{parallel}$ maps (Fig. 2). q-Space imaging was not able to detect this change. This is probably due to the already damaged white matter in widespread areas on MD maps, as shown in Fig. 5. This is in contrast with the ADC map, which still exhibits preserved regions (e.g., subcortical U-fibers). This, in turn, indicates that q-space imaging has much higher sensitivity to neuronal damage.

The visual assessment of the created maps indicated that there was relative sparing of the posterior parts of the brain, especially the occipital lobes (Fig. 4). Such occipital sparing has been pointed out in a couple of previous studies. A multi-institute study using conventional images has shown this trend [3]. A second, more recent study carried out computerized cortical thickness measurement on preclinical patients and found the trend for relative occipital sparing [21]. The results of these studies were drawn from group analysis, whereas the present observation of occipital lobe sparing was possible on an individual case basis, as illustrated in Fig. 4.

Some technical background of this q-space approach deserves comments. The effective diffusion time (i.e., $\Delta-\delta/3$) for q-space imaging is set to a much longer value than the regular clinical DWI/DTI. This leads to longer TE and thus a reduced SNR. In addition, use of extremely high b values leads to imaging data that are even more susceptible to noise. Thus, one has to use higher averaging during image acquisition. This leads to longer acquisition time, and in the present study, it took 25 min to obtain 12 slices. One can shorten the acquisition by reducing various factors, including averaging, b value increments, and gradient directions. One of the most common ways that has been used to resolve the problem is to reduce the gradient directions. For instance, a clinical study was carried out using only three orthogonal directions, which reduced the data acquisition time to 6.5 min [24]. There is, however, some criticism in reducing the MPG directions to the level where one can no longer reconstruct the tensor model.

Another limitation of "clinical" q-space imaging is that one cannot completely replicate the sequence design used in experimental conditions [6]. In the q-space formalism, the data are valid only when the following two conditions are fulfilled. The first condition is the short pulse gradient (SPG) approximation (i.e., $\delta \ll \Delta$ and δ to be infinitesimally short), and the second is the long diffusion time (i.e., $\Delta > a^2/2D$, where a is the size of the compartment, and D is the diffusion coefficient) [11]. These are not possible using a clinical scanner. Therefore, some of the clinical studies use much shorter diffusion time [24]. The advantage of this is the increase in SNR. However, it is well known that such suboptimal sequence design will lead to underestimation of compartment size [18, 19]. Our quantitative estimation of normal white matter (represented by MD_{radial}) was approximately 8.6 μm, which may thus be an underestimated value.

One of the limitations of this study includes the small number of patients. Especially, the number of preclinical patients was small (n=2), which would potentially make it difficult to assess the progressive nature of the disease. Despite such limitation, we were able to observe the statistically significant differences at some parts of brain, as indicated in Fig. 2. Another limitation of this study is the lack of direct histopathological correlation. The precise cause of the increased compartment size as measured by this technique remains unknown. There are a couple of conceivable causes, which include enlarged extracellular space due to loss of myelin/neurons and widening of perivascular space, which is known to be a unique microscopic feature of CADASIL [25]. The precise mechanism may be elucidated by future histological correlations.

In conclusion, the feasibility of demonstrating the progressive nature of white matter damage using the q-space technique in patients with CADASIL was shown. Since this method appears to be sensitive to the early damage, we believe it would aid in monitoring patients in the preclinical stage. Further longitudinal studies will be necessary to evaluate the true efficacy of this technique.

Acknowledgments This work was supported by JSPS KAKENHI Grant Number:22591348.

Conflict of interest We declare that we have no conflict of interest.

References

1. Okeda R, Arima K, Kawai M (2002) Arterial changes in CADASIL in relation to pathogenesis of diffuse myelin loss of cerebral white matter. Stroke 33:2565–2569
2. Chabriat H, Levy C, Taillia H, Iba-Zizen MT, Vahedi K, Joutel A et al (1998) Patterns of MRI lesions in CADASIL. Neurology 51:452–457
3. Singhal S, Rich P, Markus HS (2005) The spatial distribution of MR imaging abnormalities in CADASIL and their relationship to age and clinical features. AJNR Am J Neuroradiol 26:2481–2487
4. Holtmannspötter M, Peters N, Opherk C, Martin D, Herzog J, Brückmann H et al (2005) Diffusion magnetic resonance histograms as a surrogate marker and predictor of disease progression in CADASIL. Stroke 36:2559–2565
5. O'Sullivan M, Singhal S, Charlton R, Markus HS (2004) Diffusion tensor imaging of thalamus correlates with cognition in CADASIL without dementia. Neurology 62:702–707
6. Callaghan PT, Coy A, MacGowan D, Packer KJ, Zelaya FO (1991) Diffraction like effects in NMR diffusion studies of fluid in porous solids. Nature 351:467–469
7. Cory DG, Garroway AN (1990) Measurement of translational displacement probabilities by NMR. Magn Reson Med 14:435–444
8. Wu EX, Cheung MM (2010) MR diffusion kurtosis imaging for neural tissue characterization. NMR Biomed 23:836–848
9. Jensen JH, Helpern JA (2010) MRI quantification of non-Gaussian water diffusion by kurtosis analysis. NMR Biomed 23:698–710

10. Biton IE, Duncan ID, Cohen Y (2007) QSI and DTI of excised brains of the myelin-deficient rat. Magn Reson Med 58:993–1000
11. Nossin-Manor R, Duvdevani R, Cohen Y (2002) q-Space high b value diffusion MRI of hemi-crush in rat spinal cord. Magn Reson Imaging 20:231–241
12. King MD, Houseman J, Roussel SA, van Bruggen N, Williams SR, Gadian DG (1994) q-Space imaging of the brain. Magn Reson Med 32:707–713
13. King MD, Houseman J, Gadian DG, Connelly A (1997) Localized q-space imaging of the mouse brain. Magn Reson Med 38:930–937
14. Assaf Y, Mayzel-Oreg O, Gigi A, Ben-Bashat D, Mordohovitch M, Verchovsky R et al (2002) High b value q-space-analyzed diffusion MRI in vascular dementia. J Neurol Sci 203–204:235–239
15. Farrell JA, Smith SA, Gordon-Lipkin EM, Reich DS, Calabresi PA, van Zijl PC (2008) High b-value q-space diffusion-weighted MRI of the human cervical spinal cord in vivo. Magn Reson Med 59:1079–1089
16. Farrell JA, Zhang J, Jones MV, Deboy CA, Hoffman PN, Landman BA et al (2010) q-Space and conventional diffusion imaging of axon and myelin damage in the rat spinal cord after axotomy. Magn Reson Med 63:1323–1335
17. Mayzel-Oreg O, Assaf Y, Gigi A, Ben-Bashat D, Verchovsky R, Mordohovitch M et al (2007) High b-value diffusion imaging of dementia. J Neurol Sci 257:105–113
18. Biton IE, Duncan ID, Cohen Y (2007) q-Space diffusion of myelin-deficient spinal cords. Magn Reson Med 58:993–1000
19. Bar-Shir A, Avram L, Ozarslan E, Basser PJ, Cohen Y (2008) The effect of the diffusion time and pulse gradient duration ratio on the diffraction pattern and the structural information estimated from q-space diffusion MR. J Magn Reson 194:230–236
20. Ong HH, Wright AC, Wehrli SL, Souza A, Schwartz ED, Hwang SN, Wehrli FW (2008) Indirect measurement of regional axon diameter in excised mouse spinal cord with q-space imaging. Neuroimage 40:1619–1632
21. Stromillo ML, Dotti MT, Battaglini M, Mortilla M, Bianchi S, Plewnia K et al (2009) Structural and metabolic brain abnormalities in preclinical CADASIL. J Neurol Neurosurg Psychiatry 80:41–47
22. Liem MK, van der Grond J, Versluis MJ, Haan J, Webb AG, Ferrari MD et al (2010) Lenticulostriate arterial lumina are normal in CADASIL. Stroke 41:2812–2816
23. Miao Q, Paloneva T, Tuisku S, Roine S, Poyhonen M, Viitanen M, Kalimo H (2006) Arterioles of the lenticular nucleus in CADASIL. Stroke 37:2242–2247
24. Fatima Z, Motosugi U, Hori M, Ishigame K, Kumagai H, Ikenaga S et al (2010) q-Space imaging of the brain. Magn Reson Med Sci 9:109–110
25. Yamamoto Y, Ihara M, Tham C, Low RW, Slade JY, Moss T et al (2009) Neuropathological correlates of temporal pole white matter hyperintensities in CADASIL. Stroke 40:2004–2011

遺伝性脳小血管病およびその類縁疾患の診断基準の確立と治療法の研究班

区　　分	氏　名	所　　属　　等	職　　名
研究代表者	小野寺 理	新潟大学脳研究所附属生命科学リソース研究センター	教　授
研究分担者	水野 敏樹	京都府立医科大学神経内科・神経内科学	准教授
	吉田 邦広	信州大学医学部神経難病学講座・神経内科学	教　授
	豊島 靖子	新潟大学脳研究所病理学分野・神経病理学	准教授
	池内　健	新潟大学脳研究所附属生命科学リソース研究センター	教　授
研究協力者	野崎 洋明	新潟大学医学部保健学科	助　教
事　務　局	高口 久美	新潟大学脳研究所神経内科 〒951－8585　新潟市中央区旭町通1番町757 TEL:025-227-0665　FAX:025-223-6646 E-Mail:secre1@bri.niigata-u.ac.jp	秘　書
経理事務担当者	渡辺 浩匡	新潟大学医歯学系脳研究所事務室会計係　〒 951－8585　新潟市中央区旭町通1番町757 TEL:025-227-0603　FAX:025-227-0507 E-Mail:hiromasa@adm.niigata-u.ac.jp	係　長